Building Simulation 2009

Eleventh International IBPSA Conference
Glasgow, Scotland
July 27-30, 2009

ENERGY CAPTURE USING URBAN SURFACE WATER: MODELLING AND IN-SITU MEASUREMENTS

Evelyn Aparicio Medrano[1], Kees Wisse[2], and Rob Uittenbogaard[3]
[1] Delft University of Technology, Delft, The Netherlands
[2]DWA Installation and Energy Consultancy, Bodegraven, The Netherlands
[3]Deltares, Delft, The Netherlands

ABSTRACT

For engineering applications one-dimensional models of urban ponds are suitable in order to assess the energy potential for heating and cooling of buildings. This paper presents an inter-comparison of two of such models, together with in-situ measurements. Water temperatures are presented for a period of 13 diurnal cycles, as well as an inter-comparison between the heat fluxes of the two models. Stratification effects are shown by the Richardson numbers. Both models are applicable for assessment of the energy capture potential, despite different models for the heat fluxes. These conclusions are derived for discharge temperatures which deviate up to 2.5 °C from the pond temperature (pond depth = 0.4 m).

INTRODUCTION

Seasonal thermal energy storage is an effective way to reduce the energy consumption for heating and cooling of buildings. Aquifer Thermal Energy Systems (ATES) as well as underground heat exchangers are often used for cooling of buildings and as an energy source for heat pumps (Danny Harvey, 2006). However, seasonal thermal energy storage systems strongly depend on the resulting underground thermal energy balance (Wisse and Spek 2008). For aquifer systems, a zero energy balance over a number of years is necessary to prevent a short circuit between the hot and the cold well. For underground heat exchangers with a deviating balance, freezing of the heat exchanger system is possible. Energy capture using urban surface water can be used to restore the underground energy balance. Other possibilities for restoring the energy balance are asphalt pavements (Loomans et al. 2003) or dry coolers (Wisse and Spek, 2008). Using urban surface water also addresses the revival of interest in building on the water (see also de Graaf et al. 2007).

This paper concerns the modelling of the heat balance of urban surface water as well as validation using in-situ measurements. In-situ measurements have been performed in a pond near to the aquifer system of Paleiskwartier in 's Hertogenbosch (The Netherlands). This aquifer system delivers energy for heating and cooling of office buildings and apartments. During summer, the pond enables energy delivery to the hot well in case of a shortage of heat in the aquifer system.

During a period of 16 days in spring of 2008, an extensive measurement campaign has been carried out. During this period heat has been collected from the water of the pond and stored in the hot well. The measurements provided a grid with 12 temperature sensors which give spatial and temporal temperature data. The flow and temperatures of the heat exchange with the aquifer system were also monitored, as well as meteorological parameters such as: air temperature, relative humidity, wind speed, wind direction and solar radiation. The measurement period is sufficient to assess the impact of heat flux modelling as well as stratification since the temperature changes in a shallow pond have diurnal characteristics. Related to the seasonal storage the measurement period is short, but enough to give an overview of the temperature changes where heat is delivered from the pond to the underground.

The Paleiskwartier pond has been modelled using two different one-dimensional models. One model was used during the design of the pond (model A). The second model is used as a co reference (model B). The two models use different relations for the heat fluxes and this paper describes both. The inter-comparison allows us to evaluate the performance of two different models The measurements contribute to the validation of the models. We can also assess whether the models can be used for designing ponds as a heat source applications.

The paper is organized as follows. First we present the case study description, followed by the heat flux models. Subsequently the measurements and the evaluation of the simulations is given.

CASE STUDY

The studied pond is located in 's Hertogenbosch (The Netherlands). The pond is situated in the middle of the district the Paleiskwartier. The Paleiskwartier project consists of office buildings, apartments and recreational areas, accounting for 1.200 apartments and 135.000 m^2 for other

functions. The water in the pond is part of a large complex energy system, which is schematized in Figure 1. Heat and cold are delivered by a heat pump system together with the ATES technology and the pond. The pond acts as a heat source in case of shortage of heat in the ATES, due to different heating and cooling demands.

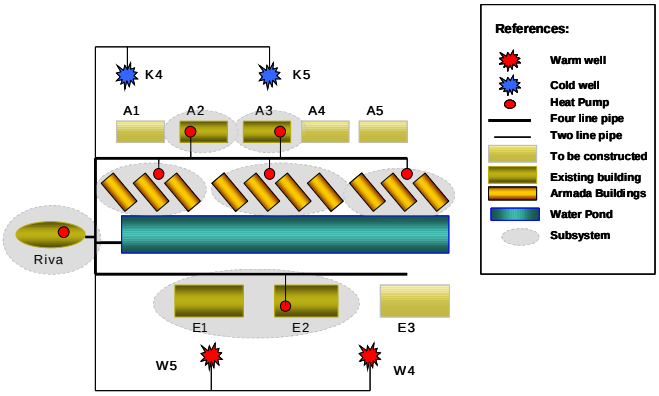

Figure 1. *General Energy System*

The water pond is 0.40 m deep, 350 m long and 32 m wide, surrounded by the buildings of the Paleiskwartier, as shown by Figure 2. The pond is constructed on top of a two level parking garage.
The water in the pond circulates from north to south, as depicted in Figure 2. In the southern part, the principal pond is connected to a secondary pond of 2 meter depth through a shallower pond. From the secondary pond a pipe guides the water back to the north extreme and into a buffer, located inside the parking garage. The buffer is connected to the ATES using a heat exchanger. From the buffer water is pumped and discharged in the fountains in the north side of the pond. The water flows from the fountain basin to the principal pond by an overflow metal weir.

The transition between the major pond and the flat pond is through a metal cascade. The flow from the flat pond to the secondary pond passes also a weir.

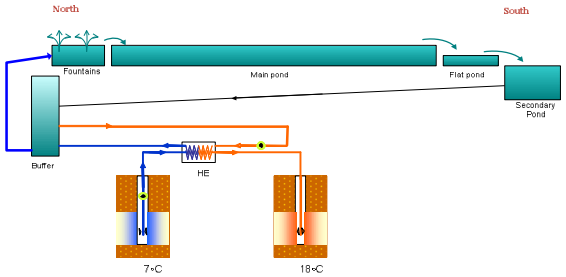

Figure 2. *Pond Water and Energy System case study*

HEAT FLUX MODEL

For comparison the design model will be named Model A, and the co reference Model B. The heat flux balance consists of the following contributions: solar radiation, net back radiation, latent heat flux, sensible heat flux and the heat loss to the underground. Table 1 shows the overview of the formulation used to build the heat flux models. The differences in the models can be summarized as follows. Model A is based on engineering formulations which are commonly used in the field of building physics. Model B is based on correlations which are convenient in the hydrodynamical field. The underlying physics of the processes are specified in more detail for Model B. For example, Model A uses a simplified model for the estimation of the net back radiation, with the water temperature, the air temperature en the relative humidity as input parameters. In Model B, the model for the net back radiation incorporates also the cloudiness (equation 11). Furthermore, Model B estimates the latent and sensible heat fluxes based on an entrainment type of approximation. Model A applies two separate empirical correlations with further simplifications for the coefficients. Another difference is the consideration of the heat flux through the bottom. Model A computes a specific flux for it while Model B includes the concrete heat content in the discretized volume. The quantitative comparison of the heat fluxes will be given in the evaluation section of this paper.

Table 1 *Heat Flux Model A and B*

Model A – Design	**Model B – Co reference**
Solar radiation (Arya, 1995)	*Solar radiation* (Arya, 1995)
$Q_{sol} = Q_{si}(1-\alpha_s)$ (1)	$Q_{sol} = Q_{si}\left(1-\alpha_s\right)$ (10)
Net back radiation (Knoll and Wagenaar,2000)	*Long wave radiation* Jacobs (1978), Prata (1996)
$Q_{netrad} = \sigma\,\varepsilon\,(T_s^4 - T_{sky}^4)$ (2)	$Q_{al} = 0.97\,\varepsilon\,\sigma\,T_a^4\left(1+0.26C\right)$ (11)
$T_{sky} = T_a - 4 - 8(1-RH)$ (3)	$\varepsilon = 1-\left(1+0.10\,w\right)\exp\left(-\sqrt{1.2+0.3w}\right)$ (12)
	$w = 46.5\,\frac{e_o}{T_a}$ (13)

	Back radiation $Q_{bl} = 0.97\sigma T_s^4$ (14) $Q_{netrad} = Q_{al} - Q_{bl}$ (14a)
Latent heat flux (Recknagel,1985) $Q_{eva} = L_v q_{eva}$ (4) $q_{eva} = h_{eva}(X_{ws} - X_{ff})$ (5) $h_{eva} = \frac{(25+19U_{10})}{3}\frac{1}{3600}$ (6)	*Latent heat flux* (Ryan et. al, 1973) $Q_{eva} = L_v\ \overline{\rho_a}\ (q_s - q_a)\left(f(U) + k_s\right)$ (15) $L_v = 2.5\cdot 10^6 - 2.3\cdot 10^3 (T_s - 273.16)$ (16) $\overline{\rho_a} = \frac{\rho_{ms} + \rho_{ma}}{2}$ (17) $f(U) = C_E\ U_{10}$ (18) $k_s = \left\{\frac{\alpha^2 g\,\Delta\rho}{\overline{\rho}_a \nu}\right\}^{\frac{1}{3}}$ (19)
Sensible heat flux (Recknagel,1991, Santamouris and Asimakopoulos, 1996) $Q_{sen} = (5.8 + 4.1U_{10})(T_s - T_a)$ (7)	*Sensible heat flux* (Ryan et. al, 1973) $Q_{sen} = \overline{\rho_a}\, c_p\ (T_s - T_a)\left(g(U) + k_s\right)$ (20) $g(U) = C_S\ U_{10}$
$Q_{bottom} = U_{bottom}(T_s - T_{underground})$ (8)	In this model the heat content of the discretized volume includes the water and the underground (concrete) portion.
$Q_{tot} = Q_{sol} - Q_{eva} - Q_{sen} - Q_{netrad} - Q_{bottom}$ (9)	$Q_{tot} = Q_{sol} + Q_{al} - Q_{bl} - Q_{eva} - Q_{sen}$ (21)

c_p = heat capacity of air [J kg^{-1} K^{-1}]

C = Cloudiness [tenths]

C_E = dimensional bulk transfer coefficient named Dalton number [-].

C_S = dimensional bulk transfer coefficient named Stanton number [-].

e_o = vapour pressure of the air [hPa].

$f(U_z)$ = wind velocity function for Latent Heat [m s^{-1}]

$g(U_z)$ = wind velocity function for Sensible Heat [m s^{-1}]

g = gravity [m s^{-2}]

h_{eva} = Wind Speed Correction [g.s^{-1}.m^{-2}]

k_s = free convection term [m s^{-1}]

L_v = latent heat [J kg $^{-1}$], model A = 2450 [J.g^{-1}.]

q_{eva} = evaporation flux [g.s^{-1}.m^{-2}]

q_s = mass ratio of vapour in saturated air [kg$_{sat}$ kg^{-1}$_{mo}$] at surface water temperature.

q_a = mass ratio of vapour in air [kg$_{vap}$ kg^{-1}$_{mo}$] at some level above the water surface.

Q_{sol} = Incident solar Radiation, [W m^{-2}],

Q_{si} = Global Solar Radiation, [W m^{-2}],

Q_{al} = Long wave Radiation, [W m^{-2}],

Q_{netrad} = Net Radiative heat flux [W m^{-2}],

Q_{eva} = Latent Heat Flux of evaporation [W m^{-2}],

Q_{sen} = Sensible Heat Flux [W m^{-2}],

Q_{bl} = back radiation [W m^{-2}]

RH = relative humidity [-]

T_{sky} = temperature of a virtual plane, accounting for the atmospheric long wave radiation [K].

T_a = air temperature [K].

T_s = surface water temperature [K].

$T_{underground}$ = Temperature in the underground [K].

U_{bottom} =Heat exchange coefficient. 2.3 [W m^{-2} K^{-1}].

U_{10} = Wind speed 10 meters from water surface [m. s $^{-1}$]

X_{ws} = Absolute humidity of saturated air for T_s [g water. kg $^{-1}$ dry air].

X_{ff} = Absolute humidity in the air [g water. kg $^{-1}$ dry air].

α_s = albedo coefficient, [-]. Model A = 0.039, Model B = 0.06

α = molecular diffusivity of air [m^2 s^{-1}]

ε = apparent emissivity of the atmosphere [-], Model A = 0.96.

σ = Stefan-Boltzman constant 5.67×10^{-8} [W m^{-2} K^{-4}]

$\overline{\rho_a}$ = average density of the air [kg m^{-3}]

ρ_{ms} = moisture density at the surface of the water [kg m^{-3}]

ρ_{ma} = moisture density at the air away from the water surface [kg m^{-3}].

$\Delta\rho$ = density difference between moist density at the surface of the water and at the air. [kg m^{-3}]

ν = viscosity of the air [m^2 s^{-1}].

MODELLING APPROACH

To model the temperature in the pond a one-dimensional approach in the longitudinal direction was followed. This is schematically shown in Figure 3 and Figure 4 for each Model A and B.

The heat flux model is solved on a hourly basis for model A, and using a five minute interval for Model B.

The meteorological data were obtained from the measurements on site.

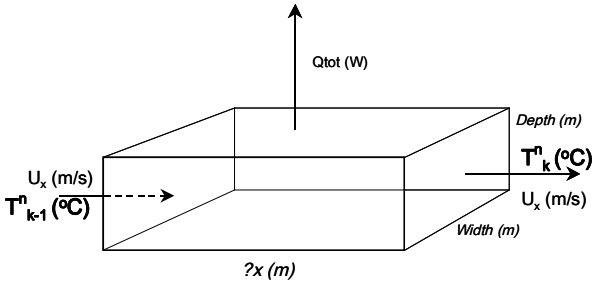

Figure 3 *Grid cell model A.*

DESIGN MODEL A

For the design model the following heat transport equation was applied:

$$\frac{\partial H}{\partial t}+\frac{\partial\left(u_i H\right)}{\partial x_i}=Q, \qquad (22)$$

The second-order term due to diffusion was not taken into account (see also equation 25). H is defined by equation 26.
The given transport equation is solved using a one-dimensional grid in the longitudinal direction of the pond. The number of grid cells in the longitudinal direction is equal to 10.
The parameters of one grid cell are given in Figure 3.

The following dicretization has been applied:

$$\frac{T_k^n-T_k^{n-1}}{\Delta t}=\frac{Q_{tot}}{\rho c_p V_j}-u_x\frac{T_k^{n-1}-T_{k-1}^{n-1}}{\Delta x}, \qquad (23)$$

Where V_j is the volume of the grid cell and

$$Q_{tot}=Q_{sol}-Q_{eva}-Q_{sens}-Q_{netrad}-Q_{bottom}, \qquad (24)$$

with Q_{tot} in [W].
The index k refers to the spatial discretization, while the index n corresponds to the discretization with respect to time. The measured temperature of the water supplied by the fountain is prescribed as a boundary condition for T_o^n. u_x is also prescribed as a boundary condition.

COREFERENCE MODEL B

The heat transport equation used by this model reads:

$$\frac{\partial H}{\partial t}+\frac{\partial\left(u_x H\right)}{\partial x}=\frac{\partial}{\partial x}\left[D\frac{\partial H}{\partial x}\right]+Q \qquad (25)$$

$$H=\rho c_p T \qquad (26)$$

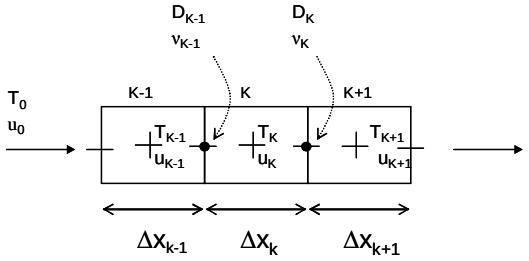

Figure 4. *Computational grid model B.*

Where H is the heat content [J m^{-3}] ρ is the density of the fluid [kg m^{-3}], c_p is the specific heat content [J kg^{-1} K^{-1}], T is the absolute temperature of water [K].

The horizontal dispersion applied is equal to:

$$D=\frac{u_* h}{6} \qquad (27)$$

Where u_* is the shear velocity [m s^{-1}], h [m] is the height of the water pond.
The following discretization has been applied:

$$\frac{\Delta x}{\Delta t}\left(T_k^{n+1}-T_k^n\right)+u_k\left(T_k^{n+1}-T_{k-1}^{n+1}\right)=\frac{D}{\Delta x}\left(2T_k^{n+1}-T_{k-1}^{n+1}-T_{k+1}^{n+1}\right)+\frac{Q_{tot}\,\Delta x}{\rho c_p V_j} \qquad (28)$$

The index k refers to the spatial discretization, while the index n corresponds to the discretization with respect to time. The measured temperature of the water supplied by the fountain and the initial velocity are prescribed as a boundary condition for T_0 and u_0.

MEASUREMENTS

The field campaign was carried out for a period of 16 days. If the first day of January 2008 is considered as day zero, the campaign was between days 146 to 161 of 2008. The energy system was operated during five days: 149,150, 153, 154 and 156. When the energy system is in operation cold water is discharged into

the buffer, after going through the heat exchanger. This is further pumped to the main pond, as schematized in figure 2.

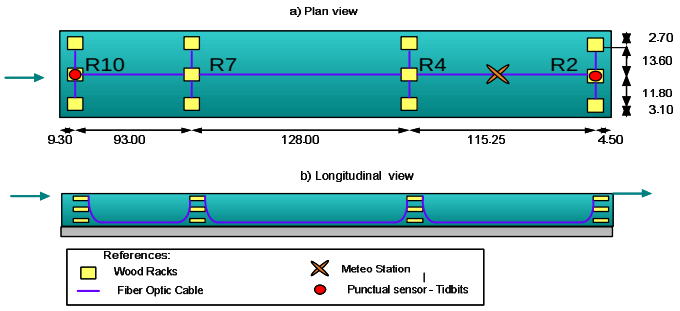

Figure 5. *Schematization of Fiber Optic Cable Set Up.*

The measurements can be divided in meteorological and water temperature measurements. The meteorological measurements consists of a meteo-station in the middle of the pond. The central meteo station was equipped with a pyranometer (S-LIB-M003, Onset, USA), air temperature and relative humidity sensors (S-THA, Onset, USA), wind speed and direction sensor (S-WCA-M003, Onset, USA) and a rain gauge (RGA-M0XX, Onset, USA). All the sensors measured with a five minutes interval.

The water temperature measurements were performed with a fiber optic cable, applying the Distributed Temperature Sensing Technique.(Selker et al, 2006). The water temperature of the pond was measured with the Sentinel DTS (Sentinel DTS-LR, London, England),and a fiber optic cable of 900 meters length arranged in three directions: longitudinal, transversal and in depth, see Figure 5. The arrangement of the cable, provides four transversal sections, one longitudinal section crossing the middle of the pond, and, at every end and intersection, temperature measurements at three different depths by using wood racks. The DTS technique allowed continuous measurement of the water temperature in the pond. The temperature was measured with a five minutes interval.

(6a)

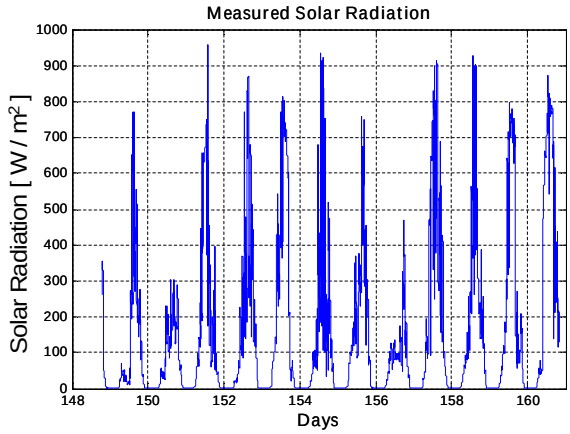

(6b)

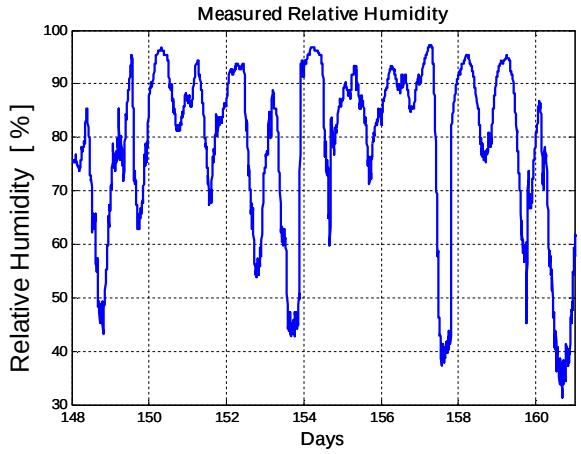

(6c)

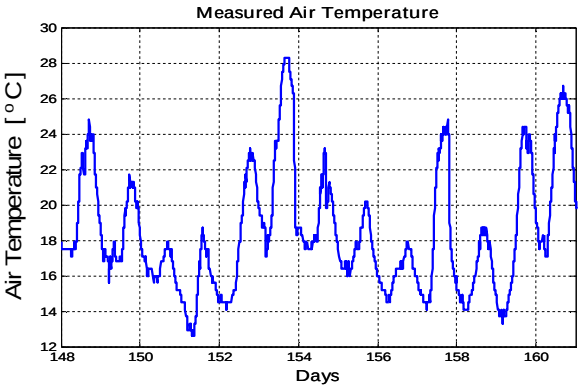

Figure 6*. (a) Measured Solar Radiation, (b) Temperature of the Air and(c) Relative Humidity.*

EVALUATION OF THE MODELS

For the simulations, the measured solar irradiation, wind speed, air temperature and relative humidity were used as input. (See Figure 6). It would be interesting to incorporate in the simulation the water temperature after the heat exchanger as an input to the system. However the pond system is interrupted by the existence of the buffer reservoir which mixes the water and changes the temperature. A simulation of the entire system is beyond the scope of this paper. The focus of the present modelling task is the temperature behaviour of the pond. Therefore the water temperature in the fountains is used as a boundary condition. The results of the measured and simulated water temperatures are given in figure 7.

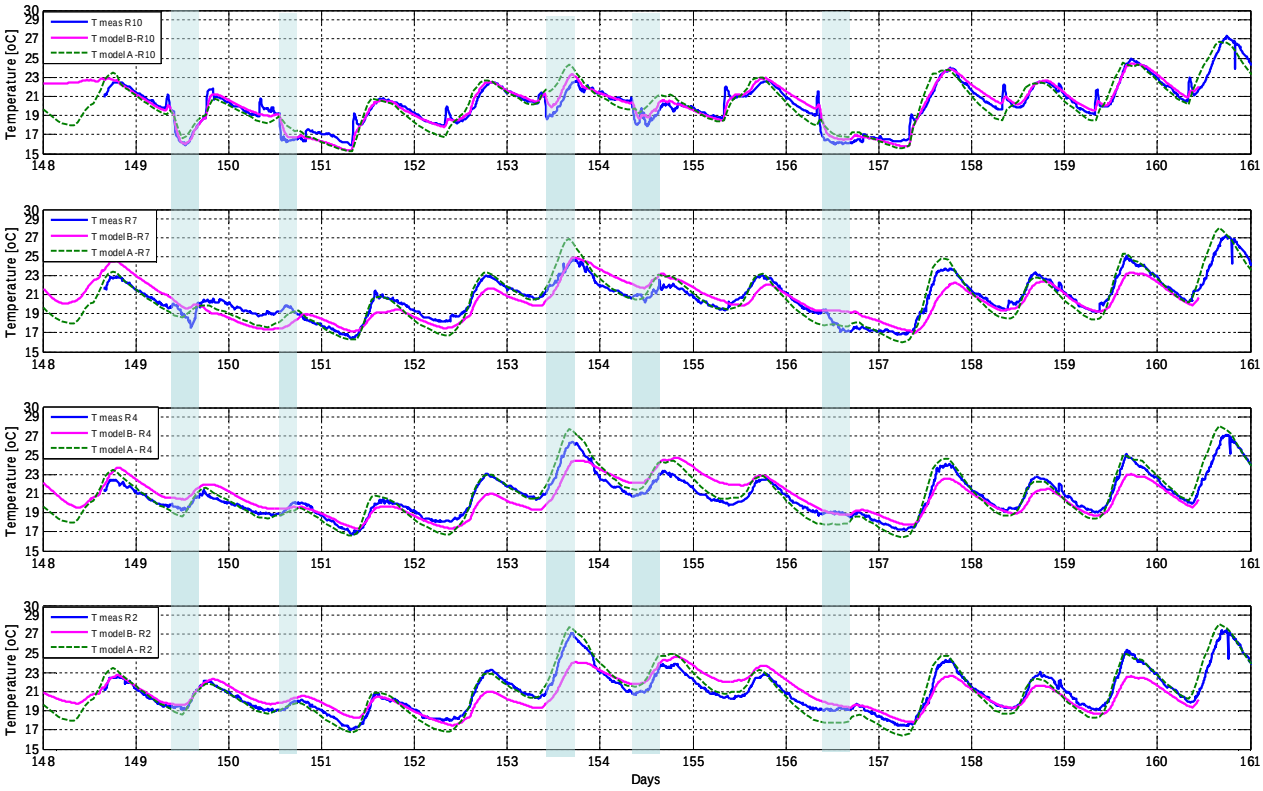

Figure 7. *Comparison Measurements and Model A and B. Blue lines show days were cold discharges occurred.*

The performance of the models has been evaluated using two coefficients: Root Mean Square Error (RMSE), and the Mean Absolute Error (MAE), the results can be seen in Table 2.

Table 2*. Performance Coefficients Model A and B*

Model A			Model B		
Position	**RMSE**	**MAE**	**Position**	**RMSE**	**MAE**
2	0.76	0.61	2	0.35	0.85
4	0.79	0.64	4	0.61	0.91
7	0.86	0.66	7	1.99	0.93
10	1.00	0.79	10	1.83	0.40

The models give good agreement with the measurements. For model A we observed that the error is larger at the beginning of the pond while for model B the opposite occurs. This is shown by the Mean Absolute Error (MAE). The peak temperatures are better simulated by Model A for the end part of the pond, while Model B performs better at the beginning of the pond. The differences in the model can be understood better when we compare each heat flux separately.

(8a)

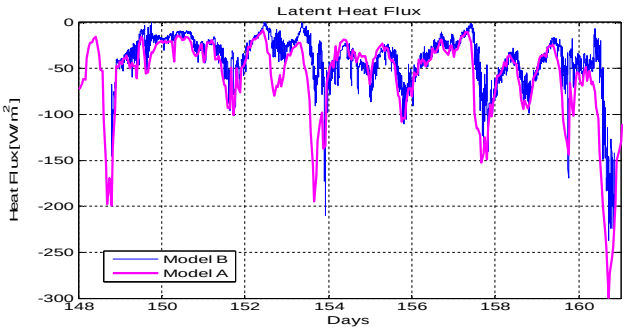

(8b)

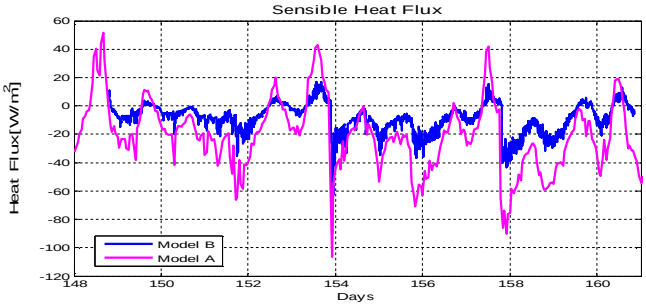

(8c)

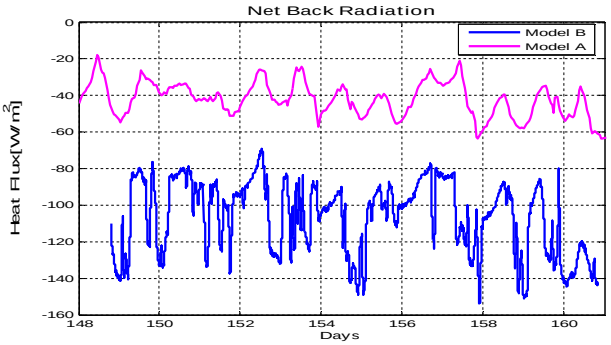

(8d)

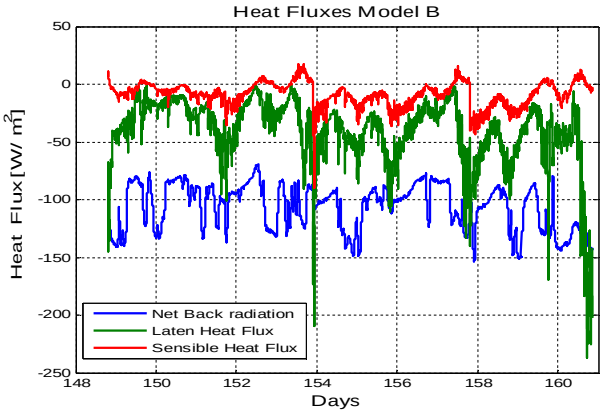

(8e)

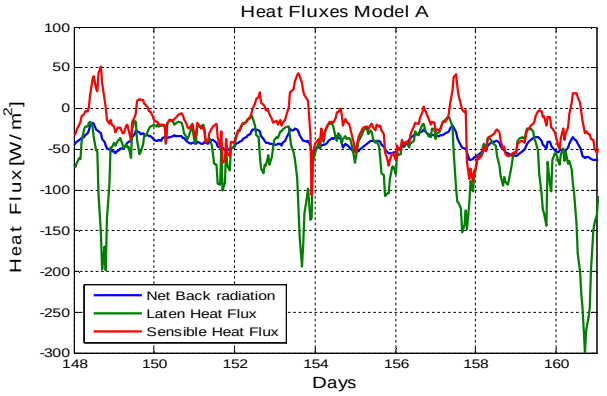

Figure 8. *Heat Fluxes comparison Model A and B.(a) Latent Heat Flux(b) Sensible Heat Flux (c) Net Back Radiation, (d) Heat Flux Balance Model B, (e) Heat Flux Balance Model A.*

Figure 8 presents the simulated heat fluxes of the pond. Model A gives a lower results for net back radiation. In model A we find about 40 [W m^{-2}] while in the Model B the fluxes are above 80 [W m^{-2}] This large difference in net long wave radiation is partially compensated by the heat loss though the concrete underground (Model A), for which Model B does not account explicitly. Instead Model B has corrected the heat content of the water column for the concrete layer below the pond. However the loss through the concrete is around 20 [W m^{-2}] which does not compensate for the 40 [W m^{-2}] difference, (figure 8c). Hence, differences in water temperatures occur.

The slower response of Model B can also be explained by the assumption made that the heat content of the volume includes the heat content of the concrete.

From the comparison of the sensible heat flux we also observe that model A computes higher peak fluxes than the model B, mainly due to the differences in the wind dependency. In spite of the differences in the formulations the latent heat flux agrees quite well.

In short we compare two different heat flux models and two different modelling approaches. However, based on water temperature measurements only we can not judge the individual heat flux correlations.

LIMITATIONS OF 1D MODELS

For the present case study stratification plays a role in the changes in temperature along the pond. The pond receives relative cold discharges from the fountains. During the measurement campaign the spatial averaged water temperature and the discharge temperature differ up to 2.5 °C. Therefore density differences can be expected to be important. Including the vertical dimension in the simulation would improve any of the temperature models presented here.

As a 1D model is by definition not able to account for stratification effects it is interesting to obtain an indication of stratification based on the measured temperatures. For that purpose we define the Richardson number in the following way:

$$Ri = -\frac{\frac{g}{\rho}\frac{\partial \rho}{\partial z}}{\left(\frac{\partial u}{\partial z}\right)^2} \tag{29}$$

$$\frac{\partial u}{\partial z} = (u_b^* + u_w^*)\frac{\ln\left(1+\frac{h}{z_o}\right)}{\kappa h} \tag{30}$$

$$\beta = \frac{1}{\rho}\frac{\partial \rho}{\partial T} \tag{31}$$

This is rewritten to the following relation:

$$Ri = -\frac{\left(\frac{g\beta}{h}\right)\left(T_{surf} - T_{bed}\right)}{\left((u_b^* + u_w^*)\frac{\ln\left(1+\frac{h}{z_o}\right)}{h\,\kappa}\right)^2} \tag{32}$$

where

$$u_b^* = \frac{Q_f}{w.h.15} \tag{33}$$

$$u_w^* = U_{10}\sqrt{\frac{\rho_a C_d}{\rho_w}} \tag{34}$$

Where Ri is the Richardson number [-], g is the gravity [m s^{-2}], ρ is the water density [kg m^{-3}], z [m] depth coordinate and u is the velocity [m s^{-1}]. β is the expansion coefficient [K^{-1}] (0.2 x 10^{-3}), u_b^* [m s^{-1}] is the shear velocity due to the discharge Q_f [m s^{-3}], u_w^* [m s^{-1}] is the shear velocity due to wind, w [m] the width of the pond, h [m] the height of pond. κ is the von Karman constant [-] (0.4), z_o [m] the roughness height (0.1 x 10^{-3}). T_{surf} and T_{bed} [K] correspond to the temperature at the surface and at the bottom of the pond. U_{10} [m s^{-1}] is the wind velocity at 10 meters above water level, C_d is the drag coefficient [-] (1.2 x 10^{-3}). For the temperature difference $(T_{surf} - T_{bed})$ we used the measurements at the top and at the bottom of Rack 4, located approximately 120 meters from the end of the pond. The Richardson numbers computed for this location are shown in Figure 9.

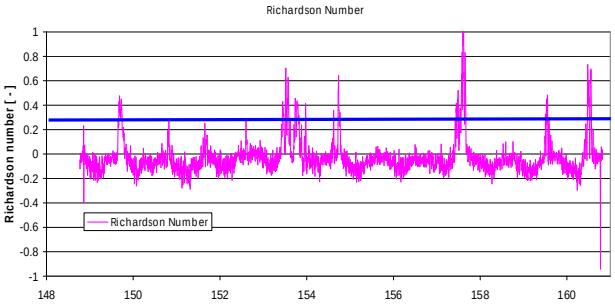

Figure 9 *Richardson number computed for a specific location on the pond 250 meters from the entrance.*

The threshold for stratification is taken as 0.3. As can be seen from Figure 9, the threshold is passed on 6 times, five of them correspond to the days where the discharge of cold water at the beginning of the pond occurs. These are the conditions that will create a stratification in the water column and therefore a 2 dimensional simulation will represent better the temperatures along the horizontal and vertical directions. Please note that for assessment of the energy potential only the temperature near the outlet of the pond is critical. The temperature near the outlet is represented by the temperature recorded at R2 (see also Figure 7).

CONCLUSIONS

In spite to have to different model approaches and different heat flux model the measured temperatures are simulated satisfactorily. The differences in each heat flux can not be assessed further in this paper. A further review of each heat flux in relation to other literature results is beyond the scope of this paper. A sensitivity analysis should focus on the long wave radiation in model A and the concrete modelling in model B. These effects give the differences as pointed out in the evaluation of the models.

When stratification of the water in the pond becomes important a 2 dimensional approach would better suite the study. Such situation can be significant if the pond will be used as a source of heat and will receive cold discharges (larger than the ones measured in this case). This can create large temperature gradients along the pond. In overall we can conclude that both models are suitable for engineering practice. These conclusions are derived for discharge temperatures which deviate up to 2.5 °C from the pond temperature (pond depth = 0.4 m).

ACKNOWLEDGEMENT

We would like to thank Essent and the Municipality of ‘s Hertogenbosch for their collaboration during the measurements campaign. We would also like to thank the TU Delft for their support during, especially to Frans van de Ven and Nick van de Giesen.

REFERENCES

Arya S.P,1998 Introduction to Micrometeorology, Second Edition (International Geophysics).

Aparicio, E, 2008. Urban Surface Water as Energy Collector & Exchanger. Master Thesis Delft University of Technology.

Danny Harvey, L.D., 2006 A handbook on low-energy buildings and district-energy systems. Earthscan/ James & James (Science Publishers) Ltd.

Jacobs, J.D., 1978: Radiation climate of Broughton Island. In: R. G. Barry and J. D. Jacobs, Energy budget studies in relation to fast-ice breakup processes in Davis Strait, *Occas. Pap. 26*,105-120. Inst. of Arctic and Alp. Res., Univ. of Colorado, Boulder, CO.

Graaf, R.E. de et al, 2007, Exploring the technical and economic feasibility of using the urban water system as a sustainable energy source, 4th DCSDE , Water and Environment Systems, 4-8 June 2007

Knoll, W.H., Wagenaar, E.J. (ed.) 2000. Handboek Installatietechniek. TVVL/ISSO (in Dutch).

Loomans et al. 2003, Design tool for the thermal energy potential of asphalt pavements. Eighth International IBPSA Conference, Eindhoven, Netherlands.

Prata, A.J.,1996. Anew long wave formula for estimating downward clear-sky radiant at the surface. Q.J.R.Meteorol. Soc..122,1127-1151.

Recknagel et al., Taschenbuch für Heizung und Klimatechnik. 1985 / 1991 R. Oldenburg Verlag, München (in German).

Ryan, P.J. Harleman, DRF & Stolzenbach, K.D.1974. Surface heat loss from cooling ponds. Water Resour. Res.,10:930:938

Santamouris and Asimakopoulos (ed.) 1996. Passive cooling of buildings. James & James (Science Publishers) Ltd.

Selker, J. S., Th´evenaz, L., Huwald, H., Mallet, A., Luxemburg, W., Van de Giesen, N., Stejskal, M., Zeman, J., Westhoff, M., and Parlange, M. B.: Distributed fiber optic temperature sensing for hydrologic systems, Water Resour. Res., 42, W12202, doi:10.1029/2006WR005326, 2006a.

Wisse, C.J. Spek, K. 2008. Climate-robust design of zero energy buildings with aquifer energy storage. In Proceedings PLEA conference 2008, University college Dublin.